



# Search for the doubly charmed baryon $\Xi_{cc}^+$ in the $\Xi_c^+ \pi^- \pi^+$ final state

LHCb collaboration<sup>†</sup>

## Abstract

A search for the doubly charmed baryon  $\Xi_{cc}^+$  is performed in the  $\Xi_c^+ \pi^- \pi^+$  invariant-mass spectrum, where the  $\Xi_c^+$  baryon is reconstructed in the  $pK^- \pi^+$  final state. The study uses proton-proton collision data collected with the LHCb detector at a centre-of-mass energy of 13 TeV, corresponding to a total integrated luminosity of  $5.4 \text{ fb}^{-1}$ . No significant signal is observed in the invariant-mass range of  $3.4\text{--}3.8 \text{ GeV}/c^2$ . Upper limits are set on the ratio of branching fractions multiplied by the production cross-section with respect to the  $\Xi_{cc}^{++} \rightarrow (\Xi_c^+ \rightarrow pK^- \pi^+) \pi^+$  decay for different  $\Xi_{cc}^+$  mass and lifetime hypotheses in the rapidity range from 2.0 to 4.5 and the transverse momentum range from 2.5 to 25  $\text{GeV}/c$ . The results from this search are combined with a previously published search for the  $\Xi_{cc}^+ \rightarrow \Lambda_c^+ K^- \pi^+$  decay mode, yielding a maximum local significance of 4.0 standard deviations around the mass of  $3620 \text{ MeV}/c^2$ , including systematic uncertainties. Taking into account the look-elsewhere effect in the  $3.5\text{--}3.7 \text{ GeV}/c^2$  mass window, the combined global significance is 2.9 standard deviations including systematic uncertainties.

Published in JHEP 12 (2021) 107

© 2022 CERN for the benefit of the LHCb collaboration. CC BY 4.0 licence.

<sup>†</sup>Authors are listed at the end of this paper.



# 1 Introduction

The quark model [1,2] predicts the existence of multiplets of baryon and meson states with a structure determined by the symmetry properties of the hadron wave functions. Baryons containing two heavy quarks provide a system for unique tests of phenomenological models and calculation techniques in quantum chromodynamics (QCD).

The first published result on a doubly charmed baryon  $\Xi_{cc}^+$  (quark content  $ccd$ ) with a mass of  $3518.7 \pm 1.7 \text{ MeV}/c^2$  was reported by the SELEX collaboration in the  $\Xi_{cc}^+ \rightarrow \Lambda_c^+ K^- \pi^+$  and  $\Xi_{cc}^+ \rightarrow p D^+ K^-$  decay modes [3,4].<sup>1</sup> However, subsequent searches for the  $\Xi_{cc}^+$  state by the FOCUS [5], BaBar [6], and Belle [7] experiments showed no evidence for the reported doubly charmed baryon. The LHCb collaboration performed a search for the  $\Xi_{cc}^+$  baryon in  $\Xi_{cc}^+ \rightarrow \Lambda_c^+ K^- \pi^+$  decays using a data sample corresponding to an integrated luminosity of  $0.65 \text{ fb}^{-1}$  [8], followed by a recent search using a data sample corresponding to  $9 \text{ fb}^{-1}$  of integrated luminosity [9], neither of which yielded any significant signal.

In 2017 the LHCb collaboration reported the first observation of the doubly charmed baryon  $\Xi_{cc}^{++}$  (quark content  $ccu$ ) in the  $\Lambda_c^+ K^- \pi^+ \pi^+$  invariant-mass spectrum [10]. Subsequently, the  $\Xi_{cc}^{++}$  baryon was confirmed in the decay mode  $\Xi_{cc}^{++} \rightarrow \Xi_c^+ \pi^+$  [11], whereas no significant signal was observed in the  $\Xi_{cc}^{++} \rightarrow D^+ p K^- \pi^+$  decay mode [12]. Recent LHCb results on the  $\Xi_{cc}^{++}$  baryon include its production measurement [13]; lifetime measurement,  $0.256_{-0.022}^{+0.024} (\text{stat}) \pm 0.014 (\text{syst}) \text{ ps}$  [14] consistent with a weak decay; and a precision mass measurement,  $3621.55 \pm 0.23 (\text{stat}) \pm 0.30 (\text{syst}) \text{ MeV}/c^2$  [15]. Searching for the isospin partner of the already well established  $\Xi_{cc}^{++}$  baryon and, more generally, studying doubly heavy baryons are of key importance for completing the baryon spectrum and shedding light on perturbative and non-perturbative QCD dynamics [16].

Various theoretical calculation techniques, such as lattice QCD [17–19], models using one light quark and two heavy quarks [20], QCD sum rules [21–25], heavy-quark effective theory [26], the bag model [27], or the relativistic quark model [28], have been applied to determine masses of the ground and excited states of the doubly charmed baryons. The majority of theoretical predictions for the masses of the  $\Xi_{cc}^{+(+)}$  ground states are in the range from 3.5 to 3.7  $\text{GeV}/c^2$  [17–46]. The mass splitting between the singly and doubly charged  $\Xi_{cc}^{+(+)}$  baryons is predicted to be small, a few  $\text{MeV}/c^2$  [47–49], due to isospin symmetry.

Most of the theoretical predictions for the lifetime of the  $\Xi_{cc}^+$  state are in the range from 40 to 250 fs [20, 29, 34, 50–55] and have large uncertainties. However, a common feature in most of these theory predictions is that the doubly charged state  $\Xi_{cc}^{++}$  is expected to have a lifetime around 2–4 times larger than the singly charged state  $\Xi_{cc}^+$  due to the effect of the destructive Pauli interference of the  $c$ -quark decay products and the valence  $u$  quark in the initial state. The  $\Xi_{cc}^+$  lifetime is further shortened due to the transition  $cd \rightarrow su$  in the  $\Xi_{cc}^+$  decays, not present in the  $\Xi_{cc}^{++}$  decays, which only proceed via the transition  $c \rightarrow su\bar{d}$  [34, 51–53]. Based on the measured lifetime of the  $\Xi_{cc}^{++}$  baryon and the theoretical predictions for the ratio of the  $\Xi_{cc}^{++}$  and  $\Xi_{cc}^+$  baryon lifetimes, the expectations for the lifetime of the singly charged state are in the range from 40 to 160 fs. This shorter lifetime makes searches for the  $\Xi_{cc}^+$  baryon more challenging.

This paper presents a search for the doubly charmed baryon  $\Xi_{cc}^+$  using the

---

<sup>1</sup>The inclusion of charge-conjugate modes is implied throughout this paper.

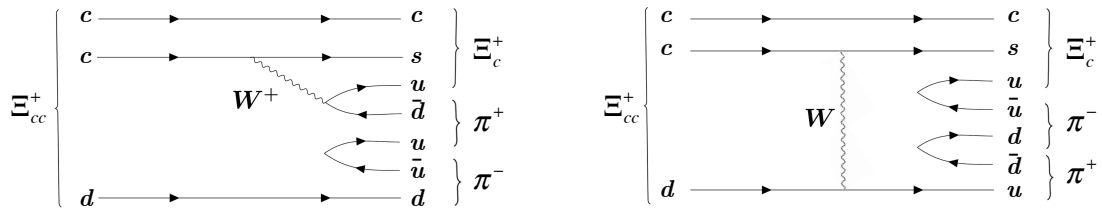


Figure 1: Examples of diagrams for the  $\Xi_{cc}^+ \rightarrow \Xi_c^+ \pi^- \pi^+$  decay.

$\Xi_{cc}^+ \rightarrow \Xi_c^+ \pi^- \pi^+$  decay mode where the  $\Xi_c^+$  candidates are reconstructed in the  $pK^- \pi^+$  final state. The dominant diagrams for this decay are shown in Fig. 1. This decay can proceed through intermediate resonances, for instance through the  $\Xi_{cc}^+ \rightarrow \Xi_c^+ (\rho^0 \rightarrow \pi^- \pi^+)$  or  $\Xi_{cc}^+ \rightarrow (\Xi_c(2645))^0 \rightarrow \Xi_c^+ \pi^- \pi^+$  decay chains. Since the final state is identical for the studied mode and the two resonant modes, all of these decays are included in the search described in this paper. As the branching fraction predictions are commonly calculated for two-body decays, the studied  $\Xi_{cc}^+ \rightarrow \Xi_c^+ \pi^- \pi^+$  final state has only an indirect prediction via its resonant decay  $\Xi_{cc}^+ \rightarrow \Xi_c^+ \rho^0$ , which is indicated as one of the most promising modes to search for the  $\Xi_{cc}^+$  baryon, alongside the  $\Xi_{cc}^+ \rightarrow \Lambda_c^+ K^- \pi^+$  and  $\Xi_{cc}^+ \rightarrow \Xi_c^0 \pi^+$  decays [16, 56, 57]. The analysis is based on  $pp$  collision data collected in 2016–2018, corresponding to an integrated luminosity of  $5.4 \text{ fb}^{-1}$ . In order to avoid experimenter’s bias, the region of the  $\Xi_c^+ \pi^- \pi^+$  invariant mass from 3.3 to 3.8  $\text{GeV}/c^2$  was not examined until the full procedure had been finalised. This range covers both the  $\Xi_{cc}^+$  mass measured by the SELEX experiment and the mass of the  $\Xi_{cc}^{++}$  baryon measured by the LHCb experiment, and most theoretical predictions.

The observed signal yield in the  $\Xi_{cc}^+ \rightarrow \Xi_c^+ \pi^- \pi^+$  decay mode is compared to that observed in the already established  $\Xi_{cc}^{++} \rightarrow \Xi_c^+ \pi^+$  channel. This enables a measurement of the ratio of production cross-section times branching fraction between the two channels or setting an upper limit on this quantity. This normalisation mode is chosen to reduce the uncertainty on the ratio of reconstruction and selection efficiencies between the two decays. The production cross-sections of the  $\Xi_{cc}^+$  and  $\Xi_{cc}^{++}$  baryons are expected to be the same [58].

The paper is organised as follows. Section 2 describes the LHCb detector and simulation, followed by Sec. 3 describing the event selection. Section 4 summarises the studies of the mass spectrum, the evaluation of the  $p$ -values and the combination with the  $\Xi_{cc}^+$  search in the  $\Lambda_c^+ K^- \pi^+$  final state. Section 5 describes the determination of the upper limit on the production cross-section multiplied by the branching fraction with respect to the normalisation channel, followed by Sec. 6 with a detailed description of the systematic uncertainties related to the upper limit evaluation. The results are presented and summarised in Secs. 7 and 8.

## 2 Detector and simulation

The LHCb detector [59, 60] is a single-arm forward spectrometer covering the pseudorapidity range  $2 < \eta < 5$ , designed for the study of particles containing  $b$  or

$c$  quarks. The detector includes a high-precision tracking system consisting of a silicon-strip vertex detector surrounding the  $pp$  interaction region [61], a large-area silicon-strip detector located upstream of a dipole magnet with a bending power of about 4 Tm, and three stations of silicon-strip detectors and straw drift tubes [62] placed downstream of the magnet. The tracking system provides a measurement of the momentum,  $p$ , of charged particles with a relative uncertainty that varies from 0.5% at low momentum to 1.0% at 200 GeV/ $c$ . The minimum distance of a track to a primary  $pp$  collision vertex (PV), the impact parameter (IP), is measured with a resolution of  $(15 + 29/p_T) \mu\text{m}$ , where  $p_T$  is the component of the momentum transverse to the beam axis, in GeV/ $c$ . Different types of charged hadrons are distinguished using information from two ring-imaging Cherenkov detectors [63]. Photons, electrons and hadrons are identified by a calorimeter system consisting of scintillating-pad and preshower detectors, an electromagnetic and a hadronic calorimeter [64]. Muons are identified by a system composed of alternating layers of iron and multiwire proportional chambers or triple-GEM detectors [65].

The online event selection is performed by a trigger [66], which consists of a hardware stage, followed by a two-level software stage, which applies a full event reconstruction. In between the two software stages, an alignment and calibration of the detector is performed in near real-time and their results are used in the trigger [67]. The same alignment and calibration information is propagated to the offline reconstruction, ensuring consistent and high-quality particle identification (PID) information between the trigger and offline software. The identical performance of the online and offline reconstruction offers the opportunity to perform physics analyses directly using candidates reconstructed in the trigger [66, 68], which is done in this analysis.

The momentum of charged particles is calibrated using samples of  $J/\psi \rightarrow \mu^+\mu^-$  and  $B^+ \rightarrow J/\psi K^+$  decays collected concurrently with the data sample used for this analysis [69, 70]. The relative accuracy of this procedure is estimated to be  $3 \times 10^{-4}$  using samples of other fully reconstructed  $b$  hadrons, and  $\Upsilon$  and  $K_S^0$  mesons.

Simulated  $\Xi_{cc}^+ \rightarrow \Xi_c^+ \pi^- \pi^+$  decays are used to optimise the signal selection and to evaluate the efficiencies used for the calculation of the upper limit on the relative production cross-section times branching fraction of the studied decay  $\Xi_{cc}^+ \rightarrow \Xi_c^+ \pi^- \pi^+$  compared to the normalisation channel  $\Xi_{cc}^{++} \rightarrow \Xi_c^+ \pi^+$ . The  $pp$  collisions are generated using PYTHIA [71] with a specific LHCb configuration [72]. A dedicated generator for doubly heavy baryon production, GENXICC2.0 [73], is used to produce the signal candidates. Decays of unstable particles are described by EVTGEN [74], in which final-state radiation is generated using PHOTOS [75]. The interaction of the generated particles with the detector, and its response, are implemented using the GEANT4 toolkit [76] as described in Ref. [77]. The  $\Xi_{cc}^+$  and  $\Xi_{cc}^{++}$  baryons are generated with a mass of 3621.4 MeV/ $c^2$ . In simulation, the decay products of the  $\Xi_{cc}^+$  and  $\Xi_{cc}^{++}$  baryons are distributed uniformly in phase space. The singly charmed  $\Xi_c^+$  decays are distributed according to a resonant model in which 55% of the  $\Xi_c^+$  decays proceed via the resonant decay  $p\bar{K}^*(892)^0$  followed by the decay of the  $\bar{K}^*(892)^0$  meson to  $K^-\pi^+$  final state [78].

### 3 Reconstruction and selection

The event selection is based on four main steps: a trigger selection, an offline selection based on sequential requirements, a multivariate-analysis (MVA) based selection, and a

removal of multiple candidates. The selection is optimised to efficiently retain the  $\Xi_{cc}^+$  signal candidates and to suppress background from random combinations of tracks and from candidates built using misidentified particles. The optimisation uses simulated events to represent the signal candidates, and the combinatorial background is represented by data with an incorrect combination of charged tracks, the same-sign pions (SSP)  $\Xi_c^+\pi^-\pi^-$  combinations. The selection of the  $\Xi_{cc}^{++} \rightarrow \Xi_c^+\pi^+$  candidates used as normalisation channel is designed to be as similar as possible to the signal channel.

This analysis uses two different trigger selections: the so-called *default trigger set*, which is used for the determination of the upper limit and is applied to both the signal and the normalisation channel in order to reduce the systematic uncertainty on the efficiency ratio between them; and the so-called *extended trigger set*, which uses more selected candidates to enhance the probability of observing a significant signal.

The offline candidates can be associated with a hardware trigger decision. The hardware trigger uses information from the muon and calorimeter systems [79]. The events can be selected by the hardware trigger either independently of the reconstructed signal or by the decay products of the signal candidate. The former category is used in the default trigger set, and additional events triggered by the decay products of the singly-charmed  $\Xi_c^+$  baryon are accepted in the extended trigger set.

In the software trigger stage of the default trigger set, the  $\Xi_c^+$  candidates must be reconstructed and accepted by a dedicated  $\Xi_c^+ \rightarrow pK^-\pi^+$  selection, which selects the  $\Xi_c^+$  baryons regardless of whether they are produced in the primary  $pp$  interaction or in a decay at a displaced vertex. All tracks from the  $\Xi_c^+$  candidates must have  $p_T$  larger than 200 MeV/ $c$ , a good track quality, and  $\chi_{\text{IP}}^2$  with respect to any PV greater than 6, where  $\chi_{\text{IP}}^2$  is defined as the difference in the vertex-fit  $\chi^2$  of a given PV reconstructed with and without the track or particle under consideration. Additionally, at least one of the three tracks must have  $p_T > 1$  GeV/ $c$  and  $\chi_{\text{IP}}^2 > 16$  and at least two of the tracks must have  $p_T > 400$  MeV/ $c$  and  $\chi_{\text{IP}}^2 > 9$ . The final state tracks are required to be reliably identified as proton, kaon or pion. Furthermore, the particles identified as protons must have a momentum of at least 10 GeV/ $c$ . The scalar sum of the  $p_T$  of the three particles must be larger than 3 GeV/ $c$ . Only the  $\Xi_c^+$  candidates with a reconstructed invariant mass in the range of 2392–2543 MeV/ $c^2$ , which corresponds to a  $\pm 75$  MeV/ $c^2$  window around the known  $\Xi_c^+$  mass [78], are retained. The  $\Xi_c^+$  candidates must have a good vertex-fit quality and point back to their associated PV, with the angle between the vector from the PV to the decay vertex of the  $\Xi_c^+$  baryon and the momentum vector of the  $\Xi_c^+$  baryon reconstructed from its decay products less than 10 mrad. The associated PV is the one that best fits the flight direction of the reconstructed candidate. The  $\Xi_c^+$  decay vertex must be displaced from the associated PV with a distance corresponding to a decay time of at least 0.15 ps. All candidates are required to pass a MatrixNet classifier [79] within the software trigger, which has been trained to identify particles with large  $p_T$ , and a decay vertex with a significant displacement from any PV. The  $\Xi_{cc}^+$  candidates are formed offline from the selected  $\Xi_c^+$  candidates combined with two oppositely charged particles identified as pions with momenta larger than 2 GeV/ $c$ ,  $p_T > 200$  MeV/ $c$  and a good track quality.

The extended trigger set includes in addition to the selection in the default trigger set two other software trigger selections for a subset of the running periods: one additional selection of the  $\Xi_{cc}^+$  candidates, similar to the default trigger selection; and the selection of the  $\Xi_c^+$  candidates using a multivariate algorithm [80, 81] trained to identify the  $\Xi_c^+$

candidates originating from any baryon decay.

The first stage of the offline selection consists of a set of sequential requirements applied before the MVA selection. All tracks are required to have momenta between 2 and 150 GeV/ $c$  and be in the pseudorapidity range from 1.5 to 5.0. The  $\Xi_{cc}^+$  candidates must have a good vertex-fit quality and point back to the associated PV. The reconstructed masses of the  $\Xi_c^+$  candidates are required to be in the range of 2450–2488 MeV/ $c^2$ , which corresponds to  $\pm 3$  times the mass resolution around its known mass of 2467.93 MeV/ $c^2$  [78]. The fiducial region is defined in the same way for both signal and normalisation modes: only the  $\Xi_{cc}^+$  and  $\Xi_{cc}^{++}$  candidates in the rapidity range from 2.0 to 4.5 and a  $p_T$  from 2.5 to 25 GeV/ $c$  are considered.

After the above requirements, the invariant mass of the final state particles originating from the  $\Xi_c^+$  vertex is recalculated under a different mass hypothesis for the SSP data in order to reveal misidentified decays. The most common background of this type is from  $D^+ \rightarrow K^- \pi^+ \pi^+$  decays where a pion is misidentified as a proton. These misidentified decays are removed by an explicit veto rejecting all candidates in a mass window of 1850–1890 MeV/ $c^2$  around the  $D^+$  mass in the  $K^- \pi^+ \pi^+$  invariant-mass spectrum for both the signal and normalisation modes. The veto removes about 20% of the background with a signal efficiency of 95%.

A multidimensional weighting procedure is used on simulated events to simultaneously correct the distributions of the  $\Xi_{cc}^{+(+)}$   $p_T$ , its  $\eta$ , and the number of tracks in the event, which are the variables where a disagreement between simulation and data is observed. The assumed  $J^P$  for the  $\Xi_{cc}^{+(+)}$  states in simulation is  $1/2^+$ . The weighting procedure uses a gradient boost algorithm [82] trained with simulated events and background-subtracted data [83] for the  $\Xi_{cc}^{++} \rightarrow \Lambda_c^+ K^- \pi^+ \pi^+$  and  $\Xi_{cc}^{++} \rightarrow \Xi_c^+ \pi^+$  decay channels. As the  $\Xi_{cc}^{++}$  and  $\Xi_{cc}^+$  baryons are isospin partners, they are expected to be produced with similar  $p_T$  and  $\eta$  spectra. Hence the same weighting procedure is applied to the simulation samples for both the signal and normalisation modes to obtain the correction weights, which are then used in the MVA training.

In order to further suppress combinatorial background and increase the signal purity, the second step of the offline selection is an MVA based selection developed using the TMVA package [84]. The MVA classifier is trained using weighted simulated events as a signal proxy and SSP combinations within the mass region of 3500–3700 MeV/ $c^2$  as a background proxy, using the candidates from the default trigger set for both simulation and the SSP data. Due to the large size of the SSP data sample, a randomly selected subset corresponding to 5% of the available data is used in the training.

The variables used in the MVA selection, ordered according to their discriminating power, are: the scalar sum of the  $p_T$  of the pions originating from the  $\Xi_{cc}^+$  candidate; the  $\chi^2$  per degree of freedom ( $\chi^2/\text{ndf}$ ) from a kinematic fit of the decay chain, with a constraint on the  $\Xi_c^+$  mass and a requirement on the  $\Xi_{cc}^+$  candidate to originate from the associated PV [85]; the ratio of the  $\Xi_c^+$  transverse momentum and the scalar sum of the  $p_T$  of the decay products of the  $\Xi_{cc}^+$  candidate; the maximum distance of closest approach (DOCA) between any pairs of the  $\Xi_{cc}^+$  daughters; the  $\chi_{\text{IP}}^2$  of the  $\Xi_{cc}^+$  candidate; the  $\chi_{\text{IP}}^2$  of the  $\Xi_c^+$  candidate; the ratio of the  $\Xi_c^+$   $\chi_{\text{IP}}^2$  and the sum of the  $\chi_{\text{IP}}^2$  of the decay products of the  $\Xi_{cc}^+$  candidate; the maximum DOCA between any pairs of the  $\Xi_c^+$  daughters; the  $\Xi_c^+$  vertex  $\chi^2/\text{ndf}$ ; the angle between the vector from the PV to the decay vertex of the  $\Xi_{cc}^+$  candidate and the momentum vector of the  $\Xi_{cc}^+$  candidate reconstructed from its decay products; the scalar sum of the  $p_T$  of the decay products of the  $\Xi_c^+$  candidate; the ratio

of the  $\Xi_c^+$  momentum to the scalar sum of the momenta of the decay products of the  $\Xi_c^+$  candidate; the vertex  $\chi^2/\text{ndf}$  of the  $\Xi_{cc}^+$  candidate; the  $\chi^2$  of the flight distance of the  $\Xi_{cc}^+$  candidate; and the  $\chi^2$  of the flight distance of the  $\Xi_c^+$  candidate.

The MVA selection is performed using a multilayer perceptron classifier [86] and the requirement on its output variable is optimised using the figure of merit introduced in Ref. [87], with a target significance of five sigma. A Kolmogorov-Smirnov test is applied on the distributions of the output variables from the training and testing samples to verify that the classifier does not show signs of overtraining. The signal efficiency of the MVA selection with respect to the selection applied before the MVA requirement is about 18% with a background rejection of about 99.9%.

Two types of multiple  $\Xi_{cc}^+$  candidates are removed after the MVA selection. First, multiple candidates for which at least one track is a clone of another track from the same candidate are removed by requiring the opening angle between any pair of tracks to be larger than 0.5 mrad. Multiple candidates which have the same set of tracks combined differently, e.g. a  $\pi^+$  from the  $\Xi_c^+$  decay swapped with the  $\pi^+$  from the  $\Xi_{cc}^+$  decay, are removed. The fraction of the first (second) type of the multiple candidates is around 3.2% (1.2%). Only one randomly chosen candidate per event is retained.

An additional requirement on the  $\Xi_c^+\pi^-\pi^-$  invariant mass is imposed after the full selection is applied, in order to separately evaluate the statistical significance of the decays that proceed through the  $\Xi_c(2645)^0$  resonance. Only the candidates where the  $\Xi_c^+\pi^-\pi^-$  invariant mass falls in the window of 2635–2660 MeV/ $c^2$ , corresponding to twice the mass resolution around the mass of the  $\Xi_c(2645)^0$  resonance [78], are considered in this selection. This gives an additional suppression of the combinatorial background, which increases the sensitivity to this resonant decay mode.

## 4 Mass distributions and signal significance

The uncertainty on the mass of the  $\Xi_{cc}^+$  candidate is reduced by measuring the difference in mass between the  $\Xi_{cc}^+$  and  $\Xi_c^+$  candidates. The measured mass of the  $\Xi_{cc}^+$  baryon is given by

$$m(\Xi_c^+\pi^+\pi^-) \equiv m([\Xi_c^+\pi^+\pi^-]_{\Xi_{cc}^+}) - m([pK^-\pi^+]_{\Xi_c^+}) + m(\Xi_c^+), \quad (1)$$

where  $m([\Xi_c^+\pi^+\pi^-]_{\Xi_{cc}^+})$  and  $m([pK^-\pi^+]_{\Xi_c^+})$  are the invariant masses of the  $\Xi_{cc}^+$  and  $\Xi_c^+$  candidates, and  $m(\Xi_c^+)$  is the known mass of the  $\Xi_c^+$  baryon [78]. The distribution of  $m(\Xi_c^+\pi^+\pi^-)$  after applying the selection and the default trigger set requirements is shown in Fig. 2. The  $\Xi_c^+\pi^-\pi^-$  data are also overlaid for comparison. The local  $p$ -value is determined as a function of the mass in steps of 1 MeV/ $c^2$ . The  $p$ -values are determined from the test statistics  $q_{\pm}$ , which are based on the ratio of likelihoods of the fit under the background-only and signal-plus-background hypotheses. The test statistics are defined similarly to the test statistic  $q_0$  defined in Ref. [88], but contrary to  $q_0$  the test statistic  $q_{\pm}$  is assigned the value  $-q_0$  when the fit yields a negative number of signal candidates, in order to obtain a smooth  $p$ -value curve also for downward fluctuations. A minimum  $p$ -value of 0.012, corresponding to a one-sided Gaussian significance of 2.3 standard deviations ( $\sigma$ ), is found at a mass of 3617 MeV/ $c^2$ . The  $p$ -value scan as a function of mass for the extended trigger set is shown in Fig. 3, for which a minimum  $p$ -value of 0.0024 at a mass of 3452 MeV/ $c^2$ , corresponding to 2.8  $\sigma$  local significance, is found. A second minimum is found at the same mass as for the default trigger set, 3617 MeV/ $c^2$ ,



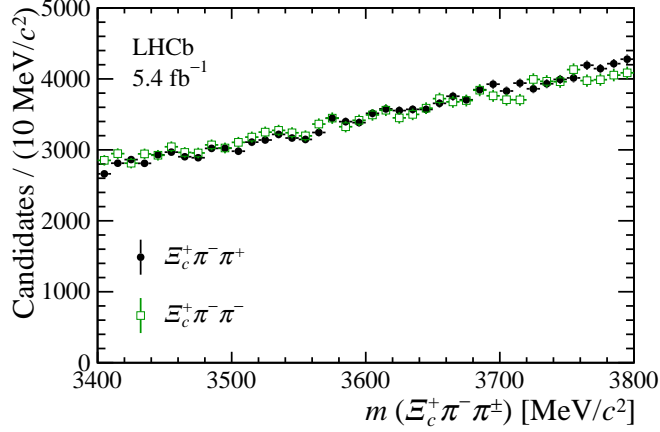


Figure 2: Invariant-mass spectrum for the  $\Xi_c^+ \pi^- \pi^+$  (black points) and the  $\Xi_c^+ \pi^- \pi^-$  (green squares) final states for the default trigger set. The  $\Xi_c^+ \pi^- \pi^-$  data are normalised to the  $\Xi_c^+ \pi^- \pi^+$  invariant-mass spectrum.

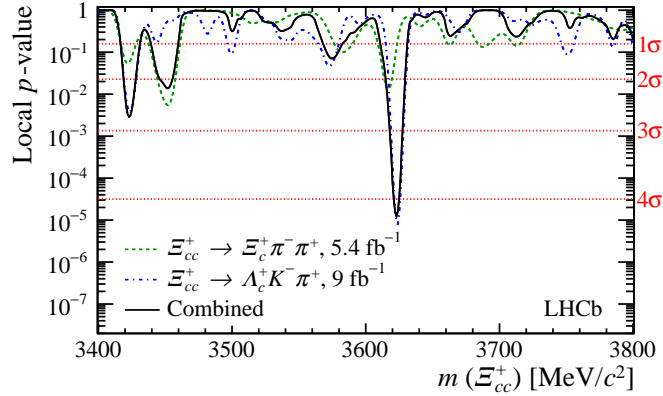


Figure 3: Local  $p$ -values as a function of the  $\Xi_{cc}^+$  invariant mass, for  $\Xi_{cc}^+$  baryon decays reconstructed in the  $\Xi_c^+ \pi^- \pi^+$  (green dashed curve) and  $\Lambda_c^+ K^- \pi^+$  (blue dash-dotted curve) modes, or combining the two modes (black solid curve). The horizontal dotted red lines represent the  $p$ -values corresponding to significances of 1, 2, 3 and 4  $\sigma$ . The extended trigger set is used for the  $\Xi_{cc}^+ \rightarrow \Xi_c^+ \pi^- \pi^+$  decay and Selection B from Ref. [9] is used for the  $\Xi_{cc}^+ \rightarrow \Lambda_c^+ K^- \pi^+$  decay. The systematic uncertainties are not taken into account.

corresponding to a  $p$ -value of 0.010 and a local significance of 2.3  $\sigma$ . Since no significant signal is observed, the mass spectrum shown in Fig. 2 is used to evaluate the upper limit on the ratio of branching fractions multiplied by the production cross-section with respect to the  $\Xi_{cc}^{++} \rightarrow (\Xi_c^+ \rightarrow p K^- \pi^+) \pi^+$  decay as described in Sec. 5. Additionally, the  $p$ -value is evaluated when the  $\Xi_c^+ \pi^-$  invariant mass is restricted around the mass of the  $\Xi_c(2645)^0$  resonance, in order to search for the resonant decay  $\Xi_{cc}^+ \rightarrow (\Xi_c(2645)^0 \rightarrow \Xi_c^+ \pi^-) \pi^+$ . No evidence for this resonant decay is found.

The results from this search are combined with the results from the search for the  $\Xi_{cc}^+$  baryon in the  $\Xi_{cc}^+ \rightarrow \Lambda_c^+ K^- \pi^+$  decay mode presented in Ref. [9]. This is performed with a combined fit to the  $\Xi_{cc}^+ \rightarrow \Xi_c^+ \pi^- \pi^+$  mass spectrum from the selection with the

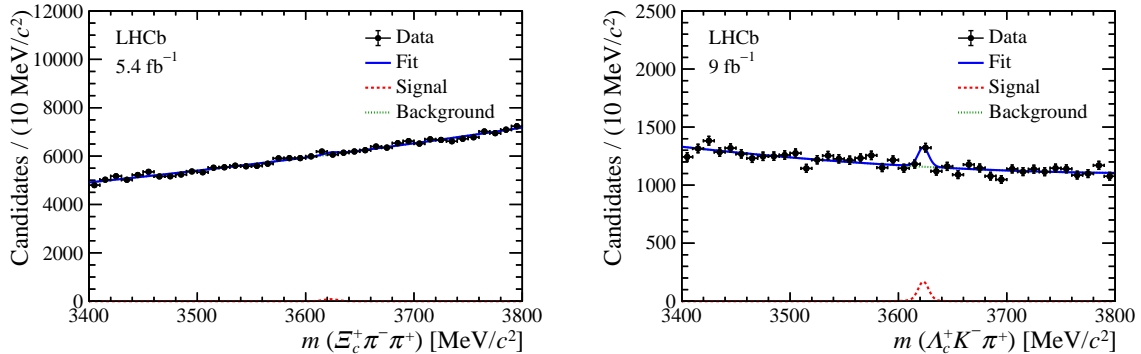


Figure 4: Invariant mass spectra for the (left)  $\Xi_c^+ \pi^- \pi^+$  and (right)  $\Lambda_c^+ K^- \pi^+$  final states. The blue solid curve represents the result of a simultaneous fit to the two spectra, with the red dashed (green dotted) curve showing the signal (background) component. The extended trigger set is used for the  $\Xi_{cc}^+ \rightarrow \Xi_c^+ \pi^- \pi^+$  decay and Selection B from Ref. [9] is used for the  $\Xi_{cc}^+ \rightarrow \Lambda_c^+ K^- \pi^+$  decay.

extended trigger set and the  $\Xi_{cc}^+ \rightarrow \Lambda_c^+ K^- \pi^+$  mass spectrum presented in Ref. [9].<sup>2</sup> The signal component is modelled with the sum of a Gaussian function and a Crystal Ball function with power-law tails on both sides [89] with a shared mean for both decay channels. An exponential function is used to describe the background contribution for the  $\Xi_{cc}^+ \rightarrow \Xi_c^+ \pi^- \pi^+$  decay and a second-order Chebyshev polynomial is used to model the background component for the  $\Xi_{cc}^+ \rightarrow \Lambda_c^+ K^- \pi^+$  decay. The parameters of the signal model are fixed to the values obtained from simulation, all fit parameters in the background model vary freely. Figure 4 shows the  $\Xi_c^+ \pi^- \pi^+$  and  $\Lambda_c^+ K^- \pi^+$  invariant-mass spectra, simultaneous unbinned extended maximum-likelihood fit with a common mass and independent signal and background yields is overlaid. The best-fit mass value is  $3623.0 \pm 1.4 \text{ MeV}/c^2$ , where the uncertainty is only statistical, and the signal yield is  $223 \pm 54$  for the  $\Xi_{cc}^+ \rightarrow \Lambda_c^+ K^- \pi^+$  decay and  $145 \pm 139$  for the  $\Xi_{cc}^+ \rightarrow \Xi_c^+ \pi^- \pi^+$  decay.

The combined  $p$ -values are based on the sum of the test statistics from the two spectra. Since compatibility with the background-only hypothesis is not unambiguously defined for fits to more than one data set, two alternative methods are used to evaluate the combined  $p$ -value as cross checks and a good agreement between the methods is found.

The local  $p$ -values are calculated as a function of mass for both decay channels individually and for the combination, and are shown in Fig. 3. The individual  $p$ -values are evaluated using the asymptotic formula described in Ref. [88] since the distribution of the test statistic  $q_{\pm}$  follows a  $\chi^2$  distribution with one degree of freedom. The combined  $p$ -values are calculated from the test statistic in two steps. The  $p$ -values above  $2.2 \times 10^{-4}$  are determined from their corresponding test statistic distributions based on 50 000 background-only pseudoexperiments. The  $p$ -values below that value are calculated using the asymptotic formula, which is well described by a  $\chi^2$ -distribution with two degrees of freedom in that regime. The minimum  $p$ -value of  $1.2 \times 10^{-5}$ , corresponding to a significance of  $4.2 \sigma$  (not including systematic uncertainties), is found at a mass of  $3623 \text{ MeV}/c^2$ .

Since the mass of the  $\Xi_{cc}^+$  baryon is unknown, the global  $p$ -value in the  $3500\text{--}3700 \text{ MeV}/c^2$  invariant-mass window is evaluated to account for the look-elsewhere effect. The global  $p$ -value is computed from 40 000 background-only pseudoexperiments, and determining

<sup>2</sup>The sample used here corresponds to the one referred to as Selection B in the referenced paper.

what fraction of them has a maximum test statistic larger than the one observed in data. The resulting combined global significance is  $3.1\sigma$  without accounting for systematic uncertainties.

Three sources of systematic uncertainties are considered when evaluating the combined  $p$ -values. The first arises from the uncertainty on the relative mass scale between the two mass spectra, which is calculated as the quadratic sum of the uncorrelated systematic uncertainties. They are the uncertainties on the  $\Lambda_c^+$  and  $\Xi_c^+$  mass and those due to the  $\Xi_{cc}^+$  mass models, resulting in an uncertainty of  $0.52\text{ MeV}/c^2$ . The second source of systematic uncertainty is due to a correction on the difference in mass resolution between simulation and data, which is estimated to be  $1.37\text{ MeV}/c^2$  for the  $\Xi_{cc}^+ \rightarrow \Xi_c^+ \pi^- \pi^+$  decay and  $0.70\text{ MeV}/c^2$  for the  $\Xi_{cc}^+ \rightarrow \Lambda_c^+ K^- \pi^+$  decay. The last source of uncertainty comes from the choice of fit model, which is evaluated from 10 000 pseudoexperiments and calculating the difference between the generated yield using an alternative mass model and the fitted yield using the default mass model. This results in a relative uncertainty in the number of signal candidates of 3.1% for the  $\Xi_{cc}^+ \rightarrow \Xi_c^+ \pi^- \pi^+$  decay and 3.3% for the  $\Xi_{cc}^+ \rightarrow \Lambda_c^+ K^- \pi^+$  decay. The evaluated combined local and global significances including the systematic uncertainties are determined to be  $4.0\sigma$  and  $2.9\sigma$ , respectively.

## 5 Normalisation and single-event sensitivity

The ratio of production cross-section times the branching fraction between the signal and the normalisation channel is defined as

$$R \equiv \frac{\sigma(\Xi_{cc}^+) \times \mathcal{B}(\Xi_{cc}^+ \rightarrow \Xi_c^+ \pi^- \pi^+)}{\sigma(\Xi_{cc}^{++}) \times \mathcal{B}(\Xi_{cc}^{++} \rightarrow \Xi_c^+ \pi^+)} = \frac{\varepsilon_{\text{norm}}}{\varepsilon_{\text{sig}}} \frac{N_{\text{sig}}}{N_{\text{norm}}} \equiv \alpha N_{\text{sig}}, \quad (2)$$

where  $\sigma(\Xi_{cc}^+)$  and  $\sigma(\Xi_{cc}^{++})$  are the production cross-sections of the  $\Xi_{cc}^+$  and  $\Xi_{cc}^{++}$  baryons, which are expected to be the same [58], and  $\mathcal{B}$  represents the corresponding branching fractions. The number of observed candidates is denoted as  $N_{\text{sig}}$  for the signal channel and  $N_{\text{norm}}$  for the normalisation channel, and the corresponding efficiencies are  $\varepsilon_{\text{sig}}$  and  $\varepsilon_{\text{norm}}$ . The factor  $\alpha$  on the right side of Eq. 2 denotes the single-event sensitivity. Since no significant signal is observed for the studied  $\Xi_{cc}^+ \rightarrow \Xi_c^+ \pi^- \pi^+$  decay, the upper limit on  $R$  is evaluated as a function of assumed  $\Xi_{cc}^+$  mass and for lifetime hypotheses of 40, 80, 120 and 160 fs.

There are two main components needed for the evaluation of  $\alpha$ , the signal yield in the normalisation channel  $N_{\text{norm}}$  and the ratio of efficiencies  $\varepsilon_{\text{norm}}/\varepsilon_{\text{sig}}$ . The invariant-mass distribution of the  $\Xi_c^+ \pi^+$  final state is shown in Fig. 5, and the signal yield is determined to be  $442 \pm 56$  using an extended unbinned maximum-likelihood fit. The signal and background mass fit models are the same as for the signal decay  $\Xi_{cc}^+ \rightarrow \Xi_c^+ \pi^- \pi^+$ .

The ratio of efficiencies between the signal and normalisation channels is determined from simulation, where the  $\Xi_{cc}^{++}$  baryon lifetime is set to 256 fs, the  $\Xi_{cc}^+$  baryon lifetime is set to 80 fs and both their masses are set to  $3621.4\text{ MeV}/c^2$ . Since the lifetime and mass of the  $\Xi_{cc}^+$  baryon are unknown, the variation of the efficiency with the lifetime and mass of the  $\Xi_{cc}^+$  baryon is also considered. There are three different corrections applied to the overall efficiency ratio: a hardware-trigger correction for possible hardware-trigger mismodelling in simulation; a correction to account for the difference in the fractions of events that are selected by different software trigger categories between simulation and

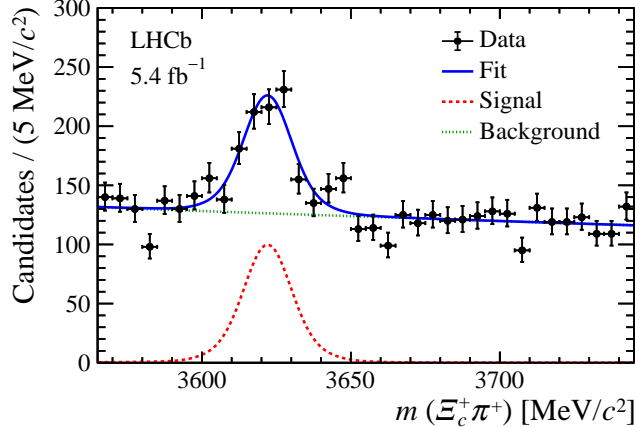


Figure 5: Invariant-mass distribution of the  $\Xi_{cc}^{++} \rightarrow \Xi_c^+ \pi^+$  candidates in the default trigger set. The blue solid line represents the total fit, the red dashed line corresponds to the signal component and the green dotted line to the background component.

Table 1: Single-event sensitivity including both statistical and systematic uncertainties evaluated for different  $\Xi_{cc}^+$  lifetime hypotheses.

Lifetime (fs)	$\alpha$
40	$0.0122 \pm 0.0018$
80	$0.0082 \pm 0.0012$
120	$0.0067 \pm 0.0010$
160	$0.0061 \pm 0.0009$

data; and finally a correction due to possible resonant contributions of the  $\rho^0$  meson to the  $\pi^- \pi^+$  spectrum. Moreover, the PID correction, determined in intervals of momentum and pseudorapidity from calibration samples, and tracking correction due to a possible mismodelling of tracking efficiency in the simulation, are evaluated for each individual track. The resulting corrected efficiency ratio is determined to be  $3.63 \pm 0.29$  where the uncertainty is dominated by the total relative systematic uncertainty of 7.9%, which is described in detail in Sec. 6. The single-event sensitivity  $\alpha$  at the lifetime hypothesis of 80 fs, including statistical and systematic uncertainties, is evaluated to be  $0.0082 \pm 0.0012$ . Given the unknown lifetime of the  $\Xi_{cc}^+$  baryon, the candidates are weighted to different lifetime hypotheses. The variation of  $\alpha$  with the lifetime, including statistical and systematic uncertainties, is summarised in Table 1. To determine the variation of the efficiency ratio with the  $\Xi_{cc}^+$  mass, five mass hypotheses are considered in addition to its default mass: 3471, 3521, 3571, 3671 and 3771  $\text{MeV}/c^2$ . A linear approximation describes the relation well and is used to determine the efficiency ratio as a function of the assumed  $\Xi_{cc}^+$  mass.

## 6 Systematic uncertainties for the upper limits

The systematic uncertainties on the ratio of efficiencies are summarised in Table 2. All systematic uncertainties on the efficiency ratio are considered to be uncorrelated. Summing them in quadrature gives a total relative systematic uncertainty of 7.9%. In addition,

Table 2: Systematic uncertainties on the ratio of efficiencies for the upper limit determination.

Category	Uncertainty on $\varepsilon_{\text{norm}}/\varepsilon_{\text{sig}}$ (%)
Tracking	2.7
PID	0.3
Hardware trigger	2.1
Simulation correction	1.7
$\Xi_{cc}^{++}$ lifetime	6.8
$\Xi_{cc}^+ \rightarrow \Xi_c^+ \rho^0$ contribution	1.1
Limited simulation sample	1.0
Combined	7.9

the systematic uncertainty on the measured signal yield of the normalisation channel is evaluated to be 2.2% and the systematic uncertainty on the measured background yield for the  $\Xi_{cc}^+ \rightarrow \Xi_c^+ \pi^- \pi^+$  decay is found to be 1.3%.

The systematic uncertainty associated with the tracking efficiency comes from the additional pion track in the signal mode that is not present in the normalisation mode, which does not cancel out in the efficiency ratio. It consists of an uncertainty on the  $\pi$  meson reconstruction efficiency due to the modelling of hadronic interactions with the detector material [90], an uncertainty from the correction method itself, and the limited size of the samples used to derive the efficiency correction. All these uncertainties are added in quadrature and the total uncertainty of the tracking efficiency is 2.7%.

The systematic uncertainty associated with the PID efficiency correction is evaluated by changing the binning scheme in the variables used for this correction, consistently for both signal and normalisation modes. The largest difference in the overall efficiency ratios between different binning schemes was found to be 0.3%, which is taken as the PID uncertainty.

The hardware-trigger decisions for the signal and normalisation modes are based on information in the event that is independent of their decay products, but there may be a correlation between this information and the kinematic properties of the doubly charmed baryons. The  $\Xi_{cc}^+$  and  $\Xi_{cc}^{++}$  baryons are expected to be produced with identical momentum spectra as they are isospin partners so the hardware trigger efficiencies are assumed to be equal for the signal and normalisation modes. However, a difference in kinematics is introduced by the selection, which is corrected for and a systematic uncertainty is evaluated for this correction. The correction is determined by comparing the ratio of the hardware trigger efficiencies in simulation before and after the selection is applied. Half of the correction, 0.9%, is assigned as a systematic uncertainty. The hardware-trigger efficiency ratio also depends on the  $\Xi_{cc}^+$  lifetime and a 1.8% systematic uncertainty is assigned to account for the unknown lifetime.

A systematic uncertainty is associated with the imperfect description of the selection variable distributions in simulation and the procedure that is used to correct them. It is evaluated from the difference in efficiency between the three-dimensional weighting in  $p_T$ ,  $\eta$  and number of tracks distributions used in the analysis, and the product of three one-dimensional weightings of the individual variables, resulting in an uncertainty of 1.7%.

The uncertainty on the measured  $\Xi_{cc}^{++}$  lifetime translates into an uncertainty on the efficiency ratio, which is evaluated by weighting the decay-time distribution in simulation to correspond to lifetimes varied by  $\pm 1\sigma$  around its measured value. The largest variation in the efficiency ratio is 6.8%, which is assigned as a systematic uncertainty.

Since it is possible that the resonant decay  $\Xi_{cc}^+ \rightarrow \Xi_c^+(\rho^0 \rightarrow \pi^-\pi^+)$  gives a significant contribution to the final state, the effect of its presence is evaluated as a systematic uncertainty. The  $\pi^-\pi^+$  invariant-mass spectrum is weighted in simulation to match the  $\rho^0$  lineshape, corresponding to the extreme case in which 100% of the companion pions would come from the  $\rho^0$  resonance, and the corresponding efficiency ratio is calculated. A correction for this potential contribution is applied by averaging the efficiency ratio with zero and 100% resonant contribution. Half of this correction, 1.1%, is assigned as systematic uncertainty.

The uncertainty on the measured signal yield of the normalisation channel is determined by considering alternative models for the signal and background shapes. A double-Gaussian function is considered as an alternative model for the signal component and a first order Chebyshev polynomial function is considered as an alternative model for the background shape. Pseudoexperiments are generated with the alternative models and fitted with the nominal model and the difference in yields is taken as a systematic uncertainty. The difference is found to be 9.7 when changing the signal model and 0.3 when changing the background model. The normalisation channel yield is thus  $N_{\text{norm}} = 442 \pm 57$  including statistical and systematic uncertainties added in quadrature.

The upper limit determination is also impacted by the background modelling. This uncertainty is estimated to be 1.3% as the maximum relative difference between the generated and fitted yields across all mass windows, where the generated yields are obtained from pseudoexperiments assuming the alternative background model.

## 7 Upper limits

The upper limits on  $R$  in Eq. 2 are determined using the CLs method [91] by using pseudoexperiments. The observed number of signal candidates ( $n_{\text{obs}}$ ), and the expected number of candidates under the background-only ( $n_{\text{b}}$ ) and signal-plus-background ( $n_{\text{sb}}$ ) hypotheses are evaluated in a mass window corresponding to twice the  $\Xi_{cc}^+$  mass resolution of  $8.9 \text{ MeV}/c^2$ . The single-event sensitivity  $\alpha$  is used to relate  $n_{\text{sb}}$  and  $R$ .

The uncertainty on the single-event sensitivity  $\alpha$  is included by sampling values from a Gaussian distribution centred at the value of  $\alpha$  with a standard deviation equal to the total uncertainty on  $\alpha$ . The systematic uncertainty on the background yield is taken into account by sampling from a Gaussian distribution centred at the number of expected background candidates with a standard deviation corresponding to 1.3% of the observed background yield. The sampled value is used as the mean of the Poisson distribution used to determine  $n_{\text{b}}$ . The effects on the upper limit from the uncertainty on the mass resolution are considered by evaluating  $n_{\text{obs}}$ ,  $n_{\text{b}}$  and  $n_{\text{sb}}$  in mass windows of different widths. The widths are determined by varying the mass resolution within its uncertainty, which is determined to be  $\pm 1.37 \text{ MeV}/c^2$  based on the difference in mass resolution between simulation and data for the normalisation mode. The study showed that the larger mass window gives a 13% larger upper limit, and is used for the evaluation of the upper limit on  $R$ .

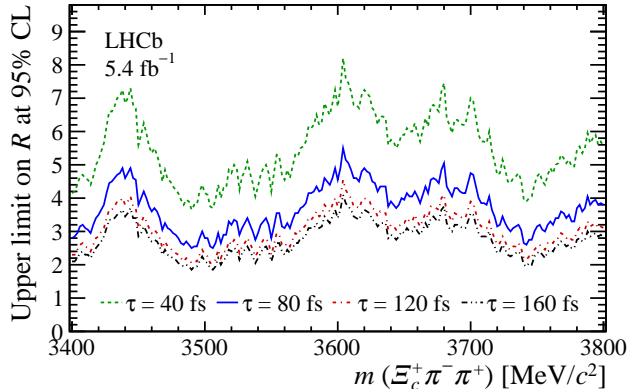


Figure 6: Upper limits on  $R$  as a function of the assumed  $\Xi_{cc}^+$  mass for four different lifetime ( $\tau$ ) hypotheses at 95% CL.

The CLs curve is determined from  $3 \times 10^5$  pseudoexperiments for each hypothetical value of  $R$  and each mass with  $2 \text{ MeV}/c^2$  steps in the  $3400\text{--}3800 \text{ MeV}/c^2$  mass window repeated for four lifetime hypotheses. The derived CLs curves are used to determine the upper limits on  $R$  at 90 and 95% confidence levels (CL). Figure 6 shows the upper limit on  $R$  as a function of mass for the four different lifetime hypotheses at 95% CL.

## 8 Conclusion

The first search for the  $\Xi_{cc}^+$  baryon in the  $\Xi_c^+ \pi^- \pi^+$  final state is presented and no significant signal is observed. The data used in this search were collected in 2016–2018, corresponding to  $5.4 \text{ fb}^{-1}$  of integrated luminosity. A minimum  $p$ -value of 0.0108 (0.0024) at a mass of 3617 (3452)  $\text{MeV}/c^2$  corresponding to  $2.3 \sigma$  ( $2.8 \sigma$ ) local significance is found for the default (extended) trigger set in the invariant-mass range of  $3400\text{--}3800 \text{ MeV}/c^2$ .

A combined fit with the  $\Xi_{cc}^+ \rightarrow \Lambda_c^+ K^- \pi^+$  decay mode is performed and the evaluated significances with systematic uncertainties included are  $4.0 \sigma$  for the local and  $2.9 \sigma$  for the global significance. The fitted mass at the minimum  $p$ -value is  $3623.0 \pm 1.4 \text{ MeV}/c^2$ , where the uncertainty is only statistical, for the simultaneous fit to the two spectra, consistent with the mass of the isospin partner  $\Xi_{cc}^{++}$ .

Upper limits on  $R$ , the relative production cross-section times branching fraction of the  $\Xi_{cc}^+ \rightarrow \Xi_c^+ \pi^- \pi^+$  decay compared to the normalisation channel  $\Xi_{cc}^{++} \rightarrow \Xi_c^+ \pi^+$ , are determined as a function of assumed  $\Xi_{cc}^+$  masses in the  $3400\text{--}3800 \text{ MeV}/c^2$  mass range for four different lifetime hypotheses. For the mid-range lifetime hypothesis of the  $\Xi_{cc}^+$  baryon of 80 fs, the upper limit on  $R$  varies between 2 and 5 at 95% CL. For the mass with the minimum  $p$ -value in the combined fit,  $3623 \text{ MeV}/c^2$ , the upper limit on  $R$  for the  $\Xi_{cc}^+$  lifetime of 80 fs is found to be 4.7 at 95% CL. Given the intriguing results presented in this paper, future searches for the  $\Xi_{cc}^+$  baryon in other decay modes using the data already collected by the LHCb detector are important to clarify the picture. Moreover, a larger data sample will be recorded in the coming years by the upgraded LHCb detector [92] which will provide more insight into doubly charmed baryons.

# Acknowledgements

We express our gratitude to our colleagues in the CERN accelerator departments for the excellent performance of the LHC. We thank the technical and administrative staff at the LHCb institutes. We acknowledge support from CERN and from the national agencies: CAPES, CNPq, FAPERJ and FINEP (Brazil); MOST and NSFC (China); CNRS/IN2P3 (France); BMBF, DFG and MPG (Germany); INFN (Italy); NWO (Netherlands); MNiSW and NCN (Poland); MEN/IFA (Romania); MSHE (Russia); MICINN (Spain); SNSF and SER (Switzerland); NASU (Ukraine); STFC (United Kingdom); DOE NP and NSF (USA). We acknowledge the computing resources that are provided by CERN, IN2P3 (France), KIT and DESY (Germany), INFN (Italy), SURF (Netherlands), PIC (Spain), GridPP (United Kingdom), RRCKI and Yandex LLC (Russia), CSCS (Switzerland), IFIN-HH (Romania), CBPF (Brazil), PL-GRID (Poland) and NERSC (USA). We are indebted to the communities behind the multiple open-source software packages on which we depend. Individual groups or members have received support from ARC and ARDC (Australia); AvH Foundation (Germany); EPLANET, Marie Skłodowska-Curie Actions and ERC (European Union); A\*MIDEX, ANR, IPhU and Labex P2IO, and Région Auvergne-Rhône-Alpes (France); Key Research Program of Frontier Sciences of CAS, CAS PIFI, CAS CCEPP, Fundamental Research Funds for the Central Universities, and Sci. & Tech. Program of Guangzhou (China); RFBR, RSF and Yandex LLC (Russia); GVA, XuntaGal and GENCAT (Spain); the Leverhulme Trust, the Royal Society and UKRI (United Kingdom).

# References

- [1] M. Gell-Mann, *A schematic model of baryons and mesons*, Phys. Lett. **8** (1964) 214.
- [2] G. Zweig, *An  $SU_3$  model for strong interaction symmetry and its breaking; Version 1* CERN-TH-401, CERN, Geneva, 1964; G. Zweig, *An  $SU_3$  model for strong interaction symmetry and its breaking; Version 2* CERN-TH-412, CERN, 1964.
- [3] SELEX collaboration, M. Mattson *et al.*, *First observation of the doubly charmed baryon  $\Xi_{cc}^+$* , Phys. Rev. Lett. **89** (2002) 112001, [arXiv:hep-ex/0208014](#).
- [4] SELEX collaboration, A. Ocherashvili *et al.*, *Confirmation of the double charm baryon  $\Xi_{cc}^+(3520)$  via its decay to  $pD^+K^-$* , Phys. Lett. **B628** (2005) 18, [arXiv:hep-ex/0406033](#).
- [5] S. P. Ratti *et al.*, *New results on  $c$ -baryons and a search for  $cc$ -baryons in FOCUS*, Nucl. Phys. Proc. Suppl. **115** (2003) 33.
- [6] BaBar collaboration, B. Aubert *et al.*, *Search for doubly charmed baryons  $\Xi_{cc}^+$  and  $\Xi_{cc}^{++}$  in BABAR*, Phys. Rev. **D74** (2006) 011103, [arXiv:hep-ex/0605075](#).
- [7] Belle collaboration, R. Chistov *et al.*, *Observation of new states decaying into  $\Lambda_c^+ K^- \pi^+$  and  $\Lambda_c^+ K_S^0 \pi^-$* , Phys. Rev. Lett. **97** (2006) 162001, [arXiv:hep-ex/0606051](#).
- [8] LHCb collaboration, R. Aaij *et al.*, *Search for the doubly charmed baryon  $\Xi_{cc}^+$* , JHEP **12** (2013) 090, [arXiv:1310.2538](#).



- [9] LHCb collaboration, R. Aaij *et al.*, *Search for the doubly charmed baryon  $\Xi_{cc}^+$* , Sci. China Phys. Mech. Astron. **63** (2020) 221062, [arXiv:1909.12273](#).
- [10] LHCb collaboration, R. Aaij *et al.*, *Observation of the doubly charmed baryon  $\Xi_{cc}^{++}$* , Phys. Rev. Lett. **119** (2017) 112001, [arXiv:1707.01621](#).
- [11] LHCb collaboration, R. Aaij *et al.*, *First observation of the doubly charmed baryon decay  $\Xi_{cc}^{++} \rightarrow \Xi_c^+ \pi^+$* , Phys. Rev. Lett. **121** (2018) 162002, [arXiv:1807.01919](#).
- [12] LHCb collaboration, R. Aaij *et al.*, *A search for  $\Xi_{cc}^{++} \rightarrow D^+ p K^- \pi^+$  decays*, JHEP **10** (2019) 124, [arXiv:1905.02421](#).
- [13] LHCb collaboration, R. Aaij *et al.*, *Measurement of  $\Xi_{cc}^{++}$  production in  $pp$  collisions at  $\sqrt{s} = 13$  TeV*, Chin. Phys. **C44** (2020) 022001, [arXiv:1910.11316](#).
- [14] LHCb collaboration, R. Aaij *et al.*, *Measurement of the lifetime of the doubly charmed baryon  $\Xi_{cc}^{++}$* , Phys. Rev. Lett. **121** (2018) 052002, [arXiv:1806.02744](#).
- [15] LHCb collaboration, R. Aaij *et al.*, *Precision measurement of the  $\Xi_{cc}^{++}$  mass*, JHEP **02** (2020) 049, [arXiv:1911.08594](#).
- [16] F. Yu *et al.*, *Discovery potentials of doubly charmed baryons*, Chin. Phys. **C42** (2018) 051001, [arXiv:1703.09086](#).
- [17] R. A. Briceno, H.-W. Lin, and D. R. Bolton, *Charmed-baryon spectroscopy from lattice QCD with  $N_f = 2 + 1 + 1$  flavors*, Phys. Rev. **D86** (2012) 094504, [arXiv:1207.3536](#).
- [18] Z. S. Brown, W. Detmold, S. Meinel, and K. Orginos, *Charmed bottom baryon spectroscopy from lattice QCD*, Phys. Rev. **D90** (2014) 094507, [arXiv:1409.0497](#).
- [19] C. Alexandrou *et al.*, *Baryon spectrum with  $N_f = 2 + 1 + 1$  twisted mass fermions*, Phys. Rev. **D90** (2014) 074501, [arXiv:1406.4310](#).
- [20] M. Karliner and J. L. Rosner, *Baryons with two heavy quarks: Masses, production, decays, and detection*, Phys. Rev. **D90** (2014) 094007, [arXiv:1408.5877](#).
- [21] D. B. Lichtenberg, R. Roncaglia, and E. Predazzi, *Mass sum rules for singly and doubly heavy flavored hadrons*, Phys. Rev. **D53** (1996) 6678, [arXiv:hep-ph/9511461](#).
- [22] J. Zhang and M. Huang, *Doubly heavy baryons in QCD sum rules*, Phys. Rev. **D78** (2008) 094007, [arXiv:0810.5396](#).
- [23] Z.-G. Wang, *Analysis of the  $\frac{1}{2}^+$  doubly heavy baryon states with QCD sum rules*, Eur. Phys. J. **A45** (2010) 267, [arXiv:1001.4693](#).
- [24] H. Chen *et al.*, *Establishing low-lying doubly charmed baryons*, Phys. Rev. **D96** (2017) 031501, [arXiv:1707.01779](#).
- [25] Z.-G. Wang, *Analysis of the doubly heavy baryon states and pentaquark states with QCD sum rules*, Eur. Phys. J. **C78** (2018) 826, [arXiv:1808.09820](#).
- [26] J. G. Korner, M. Kramer, and D. Pirjol, *Heavy baryons*, Prog. Part. Nucl. Phys. **33** (1994) 787, [arXiv:hep-ph/9406359](#).

- [27] D. He *et al.*, *Evaluation of spectra of baryons containing two heavy quarks in bag model*, Phys. Rev. **D70** (2004) 094004, [arXiv:hep-ph/0403301](#).
- [28] D. Ebert, R. N. Faustov, V. O. Galkin, and A. P. Martynenko, *Mass spectra of doubly heavy baryons in the relativistic quark model*, Phys. Rev. **D66** (2002) 014008, [arXiv:hep-ph/0201217](#).
- [29] S. Fleck and J.-M. Richard, *Baryons with double charm*, Prog. Theor. Phys. **82** (1989) 760.
- [30] B. O. Kerbikov, M. I. Polikarpov, and L. V. Shevchenko, *Multiquark masses and wave functions through a modified green function Monte Carlo method*, Nucl. Phys. **B331** (1990) 19.
- [31] S. Chernyshev, M. A. Nowak, and I. Zahed, *Heavy hadrons and QCD instantons*, Phys. Rev. **D53** (1996) 5176.
- [32] S. S. Gershtein, V. V. Kiselev, A. K. Likhoded, and A. I. Onishchenko, *Spectroscopy of doubly heavy baryons*, Phys. Rev. **D62** (2000) 054021.
- [33] C. Itoh, T. Minamikawa, K. Miura, and T. Watanabe, *Doubly charmed baryon masses and quark wave functions in baryons*, Phys. Rev. **D61** (2000) 057502.
- [34] V. V. Kiselev and A. K. Likhoded, *Baryons with two heavy quarks*, Phys. Usp. **45** (2002) 455, [arXiv:hep-ph/0103169](#).
- [35] N. Mathur, R. Lewis, and R. M. Woloshyn, *Charmed and bottom baryons from lattice nonrelativistic QCD*, Phys. Rev. **D66** (2002) 014502.
- [36] W. Roberts and M. Pervin, *Heavy baryons in a quark model*, Int. J. Mod. Phys. **A23** (2008) 2817, [arXiv:0711.2492](#).
- [37] A. Valcarce, H. Garcilazo, and J. Vijande, *Towards an understanding of heavy baryon spectroscopy*, Eur. Phys. J. **A37** (2008) 217.
- [38] T. M. Aliev, K. Azizi, and M. Savci, *Doubly heavy spin-1/2 baryon spectrum in QCD*, Nucl. Phys. **A895** (2012) 59, [arXiv:1205.2873](#).
- [39] PACS-CS collaboration, Y. Namekawa *et al.*, *Charmed baryons at the physical point in 2+1 flavor lattice QCD*, Phys. Rev. **D87** (2013) 094512, [arXiv:1301.4743](#).
- [40] Z.-F. Sun, Z.-W. Liu, X. Liu, and S.-L. Zhu, *Masses and axial currents of the doubly charmed baryons*, Phys. Rev. **D91** (2015) 094030, [arXiv:1411.2117](#).
- [41] M. Padmanath, R. G. Edwards, N. Mathur, and M. Peardon, *Spectroscopy of doubly-charmed baryons from lattice QCD*, Phys. Rev. **D91** (2015) 094502, [arXiv:1502.01845](#).
- [42] P. Pérez-Rubio, S. Collins, and G. S. Bali, *Charmed baryon spectroscopy and light flavor symmetry from lattice QCD*, Phys. Rev. **D92** (2015) 034504, [arXiv:1503.08440](#).
- [43] K.-W. Wei, B. Chen, and X.-H. Guo, *Masses of doubly and triply charmed baryons*, Phys. Rev. **D92** (2015) 076008, [arXiv:1503.05184](#).

- [44] Z.-F. Sun and M. J. Vicente Vacas, *Masses of doubly charmed baryons in the extended on-mass-shell renormalization scheme*, Phys. Rev. **D93** (2016) 094002, arXiv:1602.04714.
- [45] C. Alexandrou and C. Kallidonis, *Low-lying baryon masses using  $N_f = 2$  twisted mass clover-improved fermions directly at the physical pion mass*, Phys. Rev. **D96** (2017) 034511, arXiv:1704.02647.
- [46] Y. Liu and I. Zahed, *Heavy and strange holographic baryons*, Phys. Rev. **D96** (2017) 056027, arXiv:1705.01397.
- [47] C.-W. Hwang and C.-H. Chung, *Isospin mass splittings of heavy baryons in heavy quark symmetry*, Phys. Rev. **D78** (2008) 073013.
- [48] S. J. Brodsky, F. Guo, C. Hanhart, and U. Meißner, *Isospin splittings of doubly heavy baryons*, Phys. Lett. **B698** (2011) 251, arXiv:1101.1983.
- [49] M. Karliner and J. L. Rosner, *Isospin splittings in baryons with two heavy quarks*, Phys. Rev. **D96** (2017) 033004.
- [50] B. Guberina, B. Melić, and H. Štefančić, *Inclusive decays and lifetimes of doubly charmed baryons*, Eur. Phys. J. **C9** (1999) 213, arXiv:hep-ph/9901323.
- [51] V. V. Kiselev, A. K. Likhoded, and A. I. Onishchenko, *Lifetimes of doubly charmed baryons:  $\Xi_{cc}^+$  and  $\Xi_{cc}^{++}$* , Phys. Rev. **D60** (1999) 014007, arXiv:hep-ph/9807354.
- [52] A. K. Likhoded and A. I. Onishchenko, *Lifetimes of doubly heavy baryons*, arXiv:hep-ph/9912425.
- [53] C. Chang, T. Li, X. Li, and Y. Wang, *Lifetime of doubly charmed baryons*, Commun. Theor. Phys. **49** (2008) 993, arXiv:0704.0016.
- [54] A. V. Berezhnoy and A. K. Likhoded, *Doubly heavy baryons*, Phys. Atom. Nucl. **79** (2016) 260.
- [55] H.-Y. Cheng and Y.-L. Shi, *Lifetimes of Doubly Charmed Baryons*, Phys. Rev. **D98** (2018) 113005, arXiv:1809.08102.
- [56] Y.-J. Shi, W. Wang, Y. Xing, and J. Xu, *Weak Decays of Doubly Heavy Baryons: Multi-body Decay Channels*, Eur. Phys. J. **C78** (2018) 56, arXiv:1712.03830.
- [57] L.-J. Jiang, B. He, and R.-H. Li, *Weak decays of doubly heavy baryons:  $\mathcal{B}_{cc} \rightarrow \mathcal{B}_c V$* , Eur. Phys. J. **C78** (2018) 961, arXiv:1810.00541.
- [58] C.-H. Chang, C.-F. Qiao, J.-X. Wang, and X.-G. Wu, *Estimate of the hadronic production of the doubly charmed baryon  $\Xi_{cc}$  in the general-mass variable-flavor-number scheme*, Phys. Rev. **D73** (2006) 094022.
- [59] LHCb collaboration, A. A. Alves Jr. *et al.*, *The LHCb detector at the LHC*, JINST **3** (2008) S08005.
- [60] LHCb collaboration, R. Aaij *et al.*, *LHCb detector performance*, Int. J. Mod. Phys. **A30** (2015) 1530022, arXiv:1412.6352.

- [61] R. Aaij *et al.*, *Performance of the LHCb Vertex Locator*, JINST **9** (2014) P09007, arXiv:1405.7808.
- [62] P. d'Argent *et al.*, *Improved performance of the LHCb Outer Tracker in LHC Run 2*, JINST **12** (2017) P11016, arXiv:1708.00819.
- [63] M. Adinolfi *et al.*, *Performance of the LHCb RICH detector at the LHC*, Eur. Phys. J. **C73** (2013) 2431, arXiv:1211.6759.
- [64] C. Abellan Beteta *et al.*, *Calibration and performance of the LHCb calorimeters in Run 1 and 2 at the LHC*, arXiv:2008.11556, submitted to JINST.
- [65] A. A. Alves Jr. *et al.*, *Performance of the LHCb muon system*, JINST **8** (2013) P02022, arXiv:1211.1346.
- [66] R. Aaij *et al.*, *The LHCb trigger and its performance in 2011*, JINST **8** (2013) P04022, arXiv:1211.3055.
- [67] G. Dujany and B. Storaci, *Real-time alignment and calibration of the LHCb Detector in Run II*, J. Phys. Conf. Ser. **664** (2015) 082010.
- [68] R. Aaij *et al.*, *Tesla: an application for real-time data analysis in High Energy Physics*, Comput. Phys. Commun. **208** (2016) 35, arXiv:1604.05596.
- [69] LHCb collaboration, R. Aaij *et al.*, *Measurements of the  $\Lambda_b^0$ ,  $\Xi_b^-$ , and  $\Omega_b^-$  baryon masses*, Phys. Rev. Lett. **110** (2013) 182001, arXiv:1302.1072.
- [70] LHCb collaboration, R. Aaij *et al.*, *Precision measurement of  $D$  meson mass differences*, JHEP **06** (2013) 065, arXiv:1304.6865.
- [71] T. Sjöstrand, S. Mrenna, and P. Skands, *A brief introduction to PYTHIA 8.1*, Comput. Phys. Commun. **178** (2008) 852, arXiv:0710.3820; T. Sjöstrand, S. Mrenna, and P. Skands, *PYTHIA 6.4 physics and manual*, JHEP **05** (2006) 026, arXiv:hep-ph/0603175.
- [72] I. Belyaev *et al.*, *Handling of the generation of primary events in Gauss, the LHCb simulation framework*, J. Phys. Conf. Ser. **331** (2011) 032047.
- [73] C.-H. Chang, J.-X. Wang, and X.-G. Wu, *GENXICC2.0: An upgraded version of the generator for hadronic production of double heavy baryons  $\Xi_{cc}$ ,  $\Xi_{bc}$  and  $\Xi_{bb}$* , Comput. Phys. Commun. **181** (2010) 1144, arXiv:0910.4462.
- [74] D. J. Lange, *The EvtGen particle decay simulation package*, Nucl. Instrum. Meth. **A462** (2001) 152.
- [75] N. Davidson, T. Przedzinski, and Z. Was, *PHOTOS interface in C++: Technical and physics documentation*, Comp. Phys. Comm. **199** (2016) 86, arXiv:1011.0937.
- [76] Geant4 collaboration, J. Allison *et al.*, *Geant4 developments and applications*, IEEE Trans. Nucl. Sci. **53** (2006) 270; Geant4 collaboration, S. Agostinelli *et al.*, *Geant4: A simulation toolkit*, Nucl. Instrum. Meth. **A506** (2003) 250.

- [77] M. Clemencic *et al.*, *The LHCb simulation application, Gauss: Design, evolution and experience*, J. Phys. Conf. Ser. **331** (2011) 032023.
- [78] Particle Data Group, M. Tanabashi *et al.*, *Review of particle physics*, Phys. Rev. **D98** (2018) 030001, and 2019 update.
- [79] R. Aaij *et al.*, *Performance of the LHCb trigger and full real-time reconstruction in Run 2 of the LHC*, JINST **14** (2019) P04013, arXiv:1812.10790.
- [80] V. V. Gligorov and M. Williams, *Efficient, reliable and fast high-level triggering using a bonsai boosted decision tree*, JINST **8** (2013) P02013, arXiv:1210.6861.
- [81] T. Likhomanenko *et al.*, *LHCb topological trigger reoptimization*, J. Phys. Conf. Ser. **664** (2015) 082025.
- [82] A. Rogozhnikov, *Reweighting with Boosted Decision Trees*, J. Phys. Conf. Ser. **762** (2016) 012036, arXiv:1608.05806, [https://github.com/arogozhnikov/hep\\_ml](https://github.com/arogozhnikov/hep_ml).
- [83] M. Pivk and F. R. Le Diberder, *sPlot: A statistical tool to unfold data distributions*, Nucl. Instrum. Meth. **A555** (2005) 356, arXiv:physics/0402083.
- [84] H. Voss, A. Hoecker, J. Stelzer, and F. Tegenfeldt, *TMVA - Toolkit for multivariate data analysis with ROOT*, PoS **ACAT** (2007) 040.
- [85] W. D. Hulsbergen, *Decay chain fitting with a Kalman filter*, Nucl. Instrum. Meth. **A552** (2005) 566, arXiv:physics/0503191.
- [86] S. Haykin, *Neural networks: a comprehensive foundation, 2nd ed*, New York: Macmillan College Publishing, 1998.
- [87] G. Punzi, *Sensitivity of searches for new signals and its optimization*, eConf **C030908** (2003) MODT002, arXiv:physics/0308063.
- [88] G. Cowan, K. Cranmer, E. Gross, and O. Vitells, *Asymptotic formulae for likelihood-based tests of new physics*, Eur. Phys. J. **C71** (2011) 1554, arXiv:1007.1727, [Erratum: Eur. Phys. J. **C73** (2013) 2501].
- [89] T. Skwarnicki, *A study of the radiative cascade transitions between the Upsilon-prime and Upsilon resonances*, PhD thesis, Institute of Nuclear Physics, Krakow, 1986, DESY-F31-86-02.
- [90] LHCb collaboration, R. Aaij *et al.*, *Measurement of the track reconstruction efficiency at LHCb*, JINST **10** (2015) P02007, arXiv:1408.1251.
- [91] A. L. Read, *Modified frequentist analysis of search results (The CL(s) method)*, in *Workshop on Confidence Limits*, 81–101, 2000.
- [92] LHCb collaboration, *Framework TDR for the LHCb Upgrade: Technical Design Report*, CERN-LHCC-2012-007, 2012.









A. Ukleja<sup>36</sup>, D.J. Unverzagt<sup>17</sup>, E. Ursov<sup>83</sup>, A. Usachov<sup>32</sup>, A. Ustyuzhanin<sup>42,82</sup>, U. Uwer<sup>17</sup>,  
A. Vagner<sup>84</sup>, V. Vagnoni<sup>20</sup>, A. Valassi<sup>48</sup>, G. Valenti<sup>20</sup>, N. Valls Canudas<sup>85</sup>, M. van Beuzekom<sup>32</sup>,  
M. Van Dijk<sup>49</sup>, E. van Herwijnen<sup>83</sup>, C.B. Van Hulse<sup>18</sup>, M. van Veghel<sup>79</sup>, R. Vazquez Gomez<sup>45</sup>,  
P. Vazquez Regueiro<sup>46</sup>, C. Vázquez Sierra<sup>48</sup>, S. Vecchi<sup>21</sup>, J.J. Velthuis<sup>54</sup>, M. Veltri<sup>22,r</sup>,  
A. Venkateswaran<sup>68</sup>, M. Veronesi<sup>32</sup>, M. Vesterinen<sup>56</sup>, D. Vieira<sup>65</sup>, M. Vieites Diaz<sup>49</sup>,  
H. Viemann<sup>76</sup>, X. Vilasis-Cardona<sup>85</sup>, E. Vilella Figueras<sup>60</sup>, A. Villa<sup>20</sup>, P. Vincent<sup>13</sup>,  
F.C. Volle<sup>11</sup>, D. Vom Bruch<sup>10</sup>, A. Vorobyev<sup>38</sup>, V. Vorobyev<sup>43,v</sup>, N. Voropaev<sup>38</sup>, K. Vos<sup>80</sup>,  
R. Waldi<sup>17</sup>, J. Walsh<sup>29</sup>, C. Wang<sup>17</sup>, J. Wang<sup>5</sup>, J. Wang<sup>4</sup>, J. Wang<sup>3</sup>, J. Wang<sup>73</sup>, M. Wang<sup>3</sup>,  
R. Wang<sup>54</sup>, Y. Wang<sup>7</sup>, Z. Wang<sup>50</sup>, Z. Wang<sup>3</sup>, J.A. Ward<sup>56</sup>, H.M. Wark<sup>60</sup>, N.K. Watson<sup>53</sup>,  
S.G. Weber<sup>13</sup>, D. Websdale<sup>61</sup>, C. Weisser<sup>64</sup>, B.D.C. Westhenry<sup>54</sup>, D.J. White<sup>62</sup>,  
M. Whitehead<sup>54</sup>, A.R. Wiederhold<sup>56</sup>, D. Wiedner<sup>15</sup>, G. Wilkinson<sup>63</sup>, M. Wilkinson<sup>68</sup>,  
I. Williams<sup>55</sup>, M. Williams<sup>64</sup>, M.R.J. Williams<sup>58</sup>, F.F. Wilson<sup>57</sup>, W. Wislicki<sup>36</sup>, M. Witek<sup>35</sup>,  
L. Witola<sup>17</sup>, G. Wormser<sup>11</sup>, S.A. Wotton<sup>55</sup>, H. Wu<sup>68</sup>, K. Wyllie<sup>48</sup>, Z. Xiang<sup>6</sup>, D. Xiao<sup>7</sup>, Y. Xie<sup>7</sup>,  
A. Xu<sup>5</sup>, J. Xu<sup>6</sup>, L. Xu<sup>3</sup>, M. Xu<sup>7</sup>, Q. Xu<sup>6</sup>, Z. Xu<sup>5</sup>, Z. Xu<sup>6</sup>, D. Yang<sup>3</sup>, S. Yang<sup>6</sup>, Y. Yang<sup>6</sup>,  
Z. Yang<sup>5</sup>, Z. Yang<sup>66</sup>, Y. Yao<sup>68</sup>, L.E. Yeomans<sup>60</sup>, H. Yin<sup>7</sup>, J. Yu<sup>71</sup>, X. Yuan<sup>68</sup>, O. Yushchenko<sup>44</sup>,  
E. Zaffaroni<sup>49</sup>, M. Zavertyaev<sup>16,u</sup>, M. Zdybal<sup>35</sup>, O. Zenaiev<sup>48</sup>, M. Zeng<sup>3</sup>, D. Zhang<sup>7</sup>, L. Zhang<sup>3</sup>,  
S. Zhang<sup>71</sup>, S. Zhang<sup>5</sup>, Y. Zhang<sup>5</sup>, Y. Zhang<sup>63</sup>, A. Zharkova<sup>83</sup>, A. Zhelezov<sup>17</sup>, Y. Zheng<sup>6</sup>,  
T. Zhou<sup>5</sup>, X. Zhou<sup>6</sup>, Y. Zhou<sup>6</sup>, V. Zhovkovska<sup>11</sup>, X. Zhu<sup>3</sup>, Z. Zhu<sup>6</sup>, V. Zhukov<sup>14,40</sup>,  
J.B. Zonneveld<sup>58</sup>, Q. Zou<sup>4</sup>, S. Zucchelli<sup>20,d</sup>, D. Zuliani<sup>28</sup>, G. Zunica<sup>62</sup>.

<sup>1</sup>Centro Brasileiro de Pesquisas Físicas (CBPF), Rio de Janeiro, Brazil

<sup>2</sup>Universidade Federal do Rio de Janeiro (UFRJ), Rio de Janeiro, Brazil

<sup>3</sup>Center for High Energy Physics, Tsinghua University, Beijing, China

<sup>4</sup>Institute Of High Energy Physics (IHEP), Beijing, China

<sup>5</sup>School of Physics State Key Laboratory of Nuclear Physics and Technology, Peking University, Beijing, China

<sup>6</sup>University of Chinese Academy of Sciences, Beijing, China

<sup>7</sup>Institute of Particle Physics, Central China Normal University, Wuhan, Hubei, China

<sup>8</sup>Univ. Savoie Mont Blanc, CNRS, IN2P3-LAPP, Annecy, France

<sup>9</sup>Université Clermont Auvergne, CNRS/IN2P3, LPC, Clermont-Ferrand, France

<sup>10</sup>Aix Marseille Univ, CNRS/IN2P3, CPPM, Marseille, France

<sup>11</sup>Université Paris-Saclay, CNRS/IN2P3, IJCLab, Orsay, France

<sup>12</sup>Laboratoire Leprince-Ringuet, CNRS/IN2P3, Ecole Polytechnique, Institut Polytechnique de Paris, Palaiseau, France

<sup>13</sup>LPNHE, Sorbonne Université, Paris Diderot Sorbonne Paris Cité, CNRS/IN2P3, Paris, France

<sup>14</sup>I. Physikalisches Institut, RWTH Aachen University, Aachen, Germany

<sup>15</sup>Fakultät Physik, Technische Universität Dortmund, Dortmund, Germany

<sup>16</sup>Max-Planck-Institut für Kernphysik (MPIK), Heidelberg, Germany

<sup>17</sup>Physikalisches Institut, Ruprecht-Karls-Universität Heidelberg, Heidelberg, Germany

<sup>18</sup>School of Physics, University College Dublin, Dublin, Ireland

<sup>19</sup>INFN Sezione di Bari, Bari, Italy

<sup>20</sup>INFN Sezione di Bologna, Bologna, Italy

<sup>21</sup>INFN Sezione di Ferrara, Ferrara, Italy

<sup>22</sup>INFN Sezione di Firenze, Firenze, Italy

<sup>23</sup>INFN Laboratori Nazionali di Frascati, Frascati, Italy

<sup>24</sup>INFN Sezione di Genova, Genova, Italy

<sup>25</sup>INFN Sezione di Milano, Milano, Italy

<sup>26</sup>INFN Sezione di Milano-Bicocca, Milano, Italy

<sup>27</sup>INFN Sezione di Cagliari, Monserrato, Italy

<sup>28</sup>Università degli Studi di Padova, Università e INFN, Padova, Padova, Italy

<sup>29</sup>INFN Sezione di Pisa, Pisa, Italy

<sup>30</sup>INFN Sezione di Roma La Sapienza, Roma, Italy

<sup>31</sup>INFN Sezione di Roma Tor Vergata, Roma, Italy

<sup>32</sup>Nikhef National Institute for Subatomic Physics, Amsterdam, Netherlands

- <sup>33</sup> *Nikhef National Institute for Subatomic Physics and VU University Amsterdam, Amsterdam, Netherlands*
- <sup>34</sup> *AGH - University of Science and Technology, Faculty of Physics and Applied Computer Science, Kraków, Poland*
- <sup>35</sup> *Henryk Niewodniczanski Institute of Nuclear Physics Polish Academy of Sciences, Kraków, Poland*
- <sup>36</sup> *National Center for Nuclear Research (NCBJ), Warsaw, Poland*
- <sup>37</sup> *Horia Hulubei National Institute of Physics and Nuclear Engineering, Bucharest-Magurele, Romania*
- <sup>38</sup> *Petersburg Nuclear Physics Institute NRC Kurchatov Institute (PNPI NRC KI), Gatchina, Russia*
- <sup>39</sup> *Institute for Nuclear Research of the Russian Academy of Sciences (INR RAS), Moscow, Russia*
- <sup>40</sup> *Institute of Nuclear Physics, Moscow State University (SINP MSU), Moscow, Russia*
- <sup>41</sup> *Institute of Theoretical and Experimental Physics NRC Kurchatov Institute (ITEP NRC KI), Moscow, Russia*
- <sup>42</sup> *Yandex School of Data Analysis, Moscow, Russia*
- <sup>43</sup> *Budker Institute of Nuclear Physics (SB RAS), Novosibirsk, Russia*
- <sup>44</sup> *Institute for High Energy Physics NRC Kurchatov Institute (IHEP NRC KI), Protvino, Russia, Protvino, Russia*
- <sup>45</sup> *ICCUB, Universitat de Barcelona, Barcelona, Spain*
- <sup>46</sup> *Instituto Galego de Física de Altas Enerxías (IGFAE), Universidade de Santiago de Compostela, Santiago de Compostela, Spain*
- <sup>47</sup> *Instituto de Física Corpuscular, Centro Mixto Universidad de Valencia - CSIC, Valencia, Spain*
- <sup>48</sup> *European Organization for Nuclear Research (CERN), Geneva, Switzerland*
- <sup>49</sup> *Institute of Physics, Ecole Polytechnique Fédérale de Lausanne (EPFL), Lausanne, Switzerland*
- <sup>50</sup> *Physik-Institut, Universität Zürich, Zürich, Switzerland*
- <sup>51</sup> *NSC Kharkiv Institute of Physics and Technology (NSC KIPT), Kharkiv, Ukraine*
- <sup>52</sup> *Institute for Nuclear Research of the National Academy of Sciences (KINR), Kyiv, Ukraine*
- <sup>53</sup> *University of Birmingham, Birmingham, United Kingdom*
- <sup>54</sup> *H.H. Wills Physics Laboratory, University of Bristol, Bristol, United Kingdom*
- <sup>55</sup> *Cavendish Laboratory, University of Cambridge, Cambridge, United Kingdom*
- <sup>56</sup> *Department of Physics, University of Warwick, Coventry, United Kingdom*
- <sup>57</sup> *STFC Rutherford Appleton Laboratory, Didcot, United Kingdom*
- <sup>58</sup> *School of Physics and Astronomy, University of Edinburgh, Edinburgh, United Kingdom*
- <sup>59</sup> *School of Physics and Astronomy, University of Glasgow, Glasgow, United Kingdom*
- <sup>60</sup> *Oliver Lodge Laboratory, University of Liverpool, Liverpool, United Kingdom*
- <sup>61</sup> *Imperial College London, London, United Kingdom*
- <sup>62</sup> *Department of Physics and Astronomy, University of Manchester, Manchester, United Kingdom*
- <sup>63</sup> *Department of Physics, University of Oxford, Oxford, United Kingdom*
- <sup>64</sup> *Massachusetts Institute of Technology, Cambridge, MA, United States*
- <sup>65</sup> *University of Cincinnati, Cincinnati, OH, United States*
- <sup>66</sup> *University of Maryland, College Park, MD, United States*
- <sup>67</sup> *Los Alamos National Laboratory (LANL), Los Alamos, United States*
- <sup>68</sup> *Syracuse University, Syracuse, NY, United States*
- <sup>69</sup> *School of Physics and Astronomy, Monash University, Melbourne, Australia, associated to <sup>56</sup>*
- <sup>70</sup> *Pontifícia Universidade Católica do Rio de Janeiro (PUC-Rio), Rio de Janeiro, Brazil, associated to <sup>2</sup>*
- <sup>71</sup> *Physics and Micro Electronic College, Hunan University, Changsha City, China, associated to <sup>7</sup>*
- <sup>72</sup> *Guangdong Provincial Key Laboratory of Nuclear Science, Guangdong-Hong Kong Joint Laboratory of Quantum Matter, Institute of Quantum Matter, South China Normal University, Guangzhou, China, associated to <sup>3</sup>*
- <sup>73</sup> *School of Physics and Technology, Wuhan University, Wuhan, China, associated to <sup>3</sup>*
- <sup>74</sup> *Departamento de Física, Universidad Nacional de Colombia, Bogota, Colombia, associated to <sup>13</sup>*
- <sup>75</sup> *Universität Bonn - Helmholtz-Institut für Strahlen und Kernphysik, Bonn, Germany, associated to <sup>17</sup>*
- <sup>76</sup> *Institut für Physik, Universität Rostock, Rostock, Germany, associated to <sup>17</sup>*
- <sup>77</sup> *Eotvos Lorand University, Budapest, Hungary, associated to <sup>48</sup>*
- <sup>78</sup> *INFN Sezione di Perugia, Perugia, Italy, associated to <sup>21</sup>*
- <sup>79</sup> *Van Swinderen Institute, University of Groningen, Groningen, Netherlands, associated to <sup>32</sup>*
- <sup>80</sup> *Universiteit Maastricht, Maastricht, Netherlands, associated to <sup>32</sup>*
- <sup>81</sup> *National Research Centre Kurchatov Institute, Moscow, Russia, associated to <sup>41</sup>*

<sup>82</sup> *National Research University Higher School of Economics, Moscow, Russia, associated to* <sup>42</sup>

<sup>83</sup> *National University of Science and Technology "MISIS", Moscow, Russia, associated to* <sup>41</sup>

<sup>84</sup> *National Research Tomsk Polytechnic University, Tomsk, Russia, associated to* <sup>41</sup>

<sup>85</sup> *DS4DS, La Salle, Universitat Ramon Llull, Barcelona, Spain, associated to* <sup>45</sup>

<sup>86</sup> *University of Michigan, Ann Arbor, United States, associated to* <sup>68</sup>

<sup>a</sup> *Universidade Federal do Triângulo Mineiro (UFTM), Uberaba-MG, Brazil*

<sup>b</sup> *Hangzhou Institute for Advanced Study, UCAS, Hangzhou, China*

<sup>c</sup> *Università di Bari, Bari, Italy*

<sup>d</sup> *Università di Bologna, Bologna, Italy*

<sup>e</sup> *Università di Cagliari, Cagliari, Italy*

<sup>f</sup> *Università di Ferrara, Ferrara, Italy*

<sup>g</sup> *Università di Firenze, Firenze, Italy*

<sup>h</sup> *Università di Genova, Genova, Italy*

<sup>i</sup> *Università degli Studi di Milano, Milano, Italy*

<sup>j</sup> *Università di Milano Bicocca, Milano, Italy*

<sup>k</sup> *Università di Modena e Reggio Emilia, Modena, Italy*

<sup>l</sup> *Università di Padova, Padova, Italy*

<sup>m</sup> *Scuola Normale Superiore, Pisa, Italy*

<sup>n</sup> *Università di Pisa, Pisa, Italy*

<sup>o</sup> *Università della Basilicata, Potenza, Italy*

<sup>p</sup> *Università di Roma Tor Vergata, Roma, Italy*

<sup>q</sup> *Università di Siena, Siena, Italy*

<sup>r</sup> *Università di Urbino, Urbino, Italy*

<sup>s</sup> *MSU - Iligan Institute of Technology (MSU-IIT), Iligan, Philippines*

<sup>t</sup> *AGH - University of Science and Technology, Faculty of Computer Science, Electronics and Telecommunications, Kraków, Poland*

<sup>u</sup> *P.N. Lebedev Physical Institute, Russian Academy of Science (LPI RAS), Moscow, Russia*

<sup>v</sup> *Novosibirsk State University, Novosibirsk, Russia*

<sup>w</sup> *Department of Physics and Astronomy, Uppsala University, Uppsala, Sweden*

<sup>x</sup> *Hanoi University of Science, Hanoi, Vietnam*